# Clinical Evaluation of Indium-111-Labeled Chimeric Anti-CEA Monoclonal Antibody

Jeffrey Y.C. Wong, Gail E. Thomas, Dave Yamauchi, Lawrence E. Williams, Tamara L. Odom-Maryon, An Liu, Jose M. Esteban, Michael Neumaier, Stephanie Dresse, Anna M. Wu, F. James Primus, John E. Shively and Andrew A. Raubitschek

*Divisions of Radiation Oncology, Radioimmunotherapy, Surgery, Radiology, Biostatistics, Pathology, Molecular Biology and Immunology, City of Hope National Medical Center and Beckman Research Institute, Duarte, California; and J.W. Klinische Chemie, Universitäts-Krankenhaus Eppendorf, Hamburg, Germany*

Chimeric T84.66 (cT84.66) is a high-affinity ($1.16 \times 10^{11}\ M^{-1}$) $IgG_1$ monoclonal antibody (MAb) against carcinoembryonic antigen (CEA). This pilot trial evaluated the tumor-targeting properties, biodistribution, pharmacokinetics and immunogenicity of $^{111}$In-labeled cT84.66. **Methods:** Patients with CEA-producing metastatic malignancies were administered a single intravenous dose of 5 mCi $^{111}$In-diethylenetriaminepentaacetic acid-cT84.66. Serial blood samples, 24-hr urine collections and nuclear images were collected up to 7 days postinfusion. Human antichimeric antibody response was assessed up to 6 mo postinfusion. **Results:** Imaging of at least one known tumor site was observed in 14 of 15 (93%) patients. Seventy-four lesions were analyzed with an imaging sensitivity rate of 45.1% and a positive predictive value of 94.1%. In one patient, two additional bone metastases developed within 6 mo of antibody administration at sites initially felt to be falsely positive on scan. One patient developed a human antichimeric antibody response predominantly to the murine portion of the antibody. The antibody cleared serum with a median $T_{1/2\alpha}$ of 6.53 hr and a $T_{1/2\beta}$ of 90.87 hr. Interpatient variations in serum clearance rates were observed and were secondary to differences in clearance and metabolic rates of antibody–antigen complexes by the liver. One patient demonstrated very rapid clearance of antibody by the liver, which compromised antibody localization to the primary tumor. Antibody uptake in primary and metastatic tumors ranged from 0.5% to 10.5% injected dose/kg, resulting in estimated radiation doses ranging from 0.97 to 21.3 cGy/mCi $^{90}$Y. Antibody uptake in regional lymph nodes ranged from 1.3% to 377% injected dose/kg, resulting in estimated radiation doses ranging from 2.0 to 617 cGy/mCi $^{90}$Y. **Conclusion:** Chimeric T84.66 demonstrated tumor targeting that was comparable to that of other radiolabeled intact anti-CEA Mabs. Its immunogenicity after single administration was lower than murine Mabs. These properties make cT84.66 or a lower molecular weight derivative attractive for further evaluation as an imaging agent. These same properties also make it appropriate for future evaluation in Phase I therapy trials. Finally, a wide variation in the rate of antibody clearance was observed, with one patient demonstrating very slow clearance, resulting in the highest estimated marrow dose of the group, and one patient demonstrating unusually rapid clearance, resulting in poor antibody localization to tumor. Data from this study suggest that serum CEA levels, antibody–antigen complex clearance and, therefore, antibody clearance are influenced by both the production and clearance rates of CEA. This underscores the need to further identify, characterize and understand those factors that influence the biodistribution and clearance of radiolabeled anti-CEA antibodies to allow for better selection of patients for therapy and rational planning of radioimmunotherapy.

**Key Words:** chimeric antibody; carcinoembryonic antigen; indium-111; radioimmunotherapy; radiolabeled antibodies

**J Nucl Med 1997; 38:1951–1959**

Received Apr. 18, 1996; accepted Dec. 10, 1996.

For correspondence or reprints contact: Jeffrey Y.C. Wong, MD, Division of Radiation Oncology, City of Hope Medical Center, Duarte, CA 91010.

Radiolabeled monoclonal antibodies (MAbs) have shown promise as agents for cancer imaging and therapy. Phase I and II clinical trials involving several antibodies against tumor-associated antigens have been reported (*1–4*). Carcinoembryonic antigen (CEA) is one of the most important of these, as it is expressed in a variety of tumor types, including those arising from the gastrointestinal tract, lung and breast (*5–7*). Radiolabeled anti-CEA antibodies have been evaluated for both imaging (*7–11*) and therapy (*12*). For example, Beatty et al. (*13*) imaged 69% of primary colorectal carcinomas using $^{111}$In-labeled anti-CEA murine Mab T84.66 (mT84.66).

A majority of the clinical trials have evaluated murine-derived Mabs. Murine antibodies are recognized as foreign by the patient, which leads to the production of human antimouse antibodies (HAMAs) in as many as 50% of patients after single administration (*14,15*). HAMA production leads to rapid clearance of subsequently administered antibody (*16,17*). To improve this situation, investigators have engineered chimeric (human and mouse) and humanized antibodies (*18–22*), which has reduced immunogenicity. For these reasons, a chimeric version of the anti-CEA antibody mT84.66 was constructed and evaluated in a pilot pretherapy imaging trial.

## MATERIALS AND METHODS

### Antibody Production and Conjugation

Chimeric T84.66 (cT84.66) is an intact $IgG_1$ antibody derived from murine T84.66, an $IgG_1$ Mab developed at the City of Hope with high specificity and affinity for CEA (*23,24*). Chimeric T84.66 recognizes the A3 B3 domain of CEA and has little cross reactivity with normal tissues. The affinity constant of cT84.66 ($1.16 \times 10^{11}\ M^{-1}$) is comparable to that of the murine antibody ($1.25 \times 10^{11}\ M^{-1}$) (*25*). For this study, purified antibody was conjugated to the isothiocyanatobenzyl diethylenetriaminepentaacetic acid (DTPA) chelate of Sumerdon et al. (*26*). Details of the production and characterization of cT84.66 have been previously reported (*27,28*).

The final vialed lot of purified antibody conjugate used in this study met standards set by the Food and Drug Administration guidelines. An Investigational New Drug application for $^{111}$In-labeled cT84.66 is currently on file with the Food and Drug Administration.

### Radiolabeling of Antibody

Radiolabeling was performed by incubating the cT84.66–DTPA conjugate with $^{111}$In at a ratio of 1 mCi to 1 mg for 45 min at room temperature, and the reaction was stopped by the addition of 0.01 *M* sodium-EDTA. The reaction mixture was then purified by size-exclusion high-performance liquid chromatography (HPLC) (TSK-G3000 column) and diluted in normal saline with 1% human serum albumin to a total volume of 50 ml. Each dose was tested for

endotoxin by limulus amebocyte lysate assay and isotope binding by instant thin-layer chromatography. For all administered doses, radiolabeling of >90% and endotoxin levels of <1 unit/ml were demonstrated. Immunoreactivity by solid-phase CEA radioimmunoassay was consistently >95%. Preclinical human serum stability testing demonstrated <4% of $^{111}$In activity dissociating from the antibody up to 216 hr.

Preclinical murine antibody biodistribution studies of $^{111}$In-labeled cT84.66–DTPA demonstrated targeting to CEA-producing colon carcinoma xenografts (LS174T) and normal organ biodistributions that were comparable to other intact $^{111}$In-labeled anti-CEA antibodies. Tumor uptakes in the range of 50%–70% injected dose (ID)/g at 48–72 hr postinfusion were observed. Yttrium-90-DTPA–cT84.66 and $^{111}$In-DTPA–cT84.66 biodistributions were similar in the mouse model (*29*).

### Clinical Trial Design

The objectives of this pilot study were to evaluate the tumor-targeting properties, immunogenicity, pharmacokinetics and safety of administration of cT84.66. Patients were 18 yr of age or older and had evidence of CEA-producing metastatic disease based on an elevated serum CEA or positive staining on CEA immunohistochemistry of tumor biopsies. The following studies were performed before antibody administration: complete blood count and platelet count with differential, SMA-18, urinalysis, pregnancy test if indicated, plasma CEA levels, serum for human antichimeric antibody (HACA) response (in patients with previous exposure to murine or chimeric antibodies), CT scans of relevant anatomic locations corresponding to areas of metastatic or suspected metastatic disease, chest x-irradiation and electrocardiogram. If clinically indicated, bone scan, barium enema or colonoscopy was performed to assess disease location and extent. All blood studies were performed at least 2 wk before infusion, and all radiologic studies were performed at least 6 wk before antibody infusion. All patients had adequate renal and hepatic function before antibody infusion.

Chimeric T84.66 was radiolabeled with $^{111}$In at a ratio of 5 mCi $^{111}$In to 5 mg of antibody. A 100-$\mu$g test dose was first administered intravenously and was followed 15 min later by the remainder of the antibody delivered over approximately 25 min. Blood samples were taken at 30 min, at 1, 2 and 6 hr and at each scan time. Twenty-four-hour urine collections were done daily for 5 consecutive days. Spot planar and whole-body imaging studies were performed at 6, 24 and 48 hr and at 4–7 days after antibody administration using a camera with SPECT capability. SPECT scans were performed at 48 hr and at 4–5 days.

In selected cases, patients had planned surgical exploration within 2 wk after antibody infusion. Biopsies and resection of tumor and adjacent structures were done as medically indicated. Indium-111 content of resected tissues was determined on a gamma counter with a window setting of 150–500 keV, expressing results, corrected for decay, as the % ID per kg of tissue.

### Imaging Analysis

Imaging analysis was performed on a lesion-by-lesion basis. All scans were read in a blinded fashion by a nuclear medicine radiologist experienced in antibody imaging. Scan results were then compared to known sites of disease, as defined by sites of >1.0 cm on CT scans or on other conventional radiologic studies, sites imaged on bone scan or sites identified at surgery that were histologically positive for cancer. Lesions were then scored as either true-positive (TP), false-negative (FN), false-positive (FP) or true-negative (TN). Photopenic areas in the liver were not considered to be positive lesions.

### Statistical Analysis

Sensitivity and positive predictive value (PPV) were calculated using the standard statistical formulas (*30*). Exact 95% binomial confidence intervals were calculated. Specificity (TN/TN + FP) and negative predictive value (TN/TN + FN) were not calculated in this analysis because the sampling of nonmalignant tissue was not routine in this study.

### Analysis of Human Antichimeric Antibody Response

The serum HACA response to cT84.66 and cT84.66–DTPA was assayed before infusion, at 2 wk postinfusion and at 1, 3 and 6 mo postinfusion using a double-capture, solid-phase quantitative radioimmunoassay, similar to that published by LoBuglio et al. (*20*). Briefly, patients' sera were diluted 1:4 or 1:5 in normal saline, and 100 $\mu$l of each dilution were pipetted into quadruplicate glass tubes. To each tube, 100 $\mu$l $^{111}$In-labeled cT84.66 (approximately 100,000 cpm) were added. Polystyrene beads coated with cT84.66 or cT84.66–DTPA were then added to the tubes, incubated at room temperature for 90 min and washed. The beads were counted on a gamma counter. Serial dilutions of a goat antihuman Fc preparation of known concentration were used to generate a standard curve from 12.5 to 200 ng/ml 1% BSA in PBS, which was used as a negative control. A sample was scored positive if it was >12.5 ng/ml.

To further define and characterize the HACA response, competitive inhibition studies with excess cT84.66, cT84.66–DTPA, mT84.66, mT84.66-DTPA normal human IgG and normal human IgG–DTPA were performed. For inhibition studies, 50 $\mu$l of competing agent at 10 $\mu$g/ml were added to 50 $\mu$l of 1:1 diluted serum. Human antichimeric antibody radioimmunoassays were then performed as described above.

### Pharmacokinetic Analysis and Dosimetry Estimates

Blood and urine samples were counted for $^{111}$In activity on a gamma counter and were also processed on a HPLC size-exclusion Superose 6 column. In a lowest-order modeling analysis, serum kinetics were analyzed for all 15 patients using a two-compartmental model fit of each patient's time against blood and urine radioactivity curve. Fits were performed using ADAPT II software (*31*). For modeling, data points were corrected for decay and were equally weighted.

In nine patients, all nuclear scans were digitally stored for later analysis, making whole-body and normal organ absorbed radiation doses estimates possible from serial $^{111}$In scans of the whole body and local anatomical areas. Parallel-opposed images were used to construct the geometric mean uptake as a function of time for those organs seen in both projections. Otherwise, single-view images were acquired. All resultant curves on $^{111}$In activity against time were corrected for background and patient attenuation. Attenuation was estimated using a separate series of experiments involving gamma camera efficiency in counting a planar $^{111}$In phantom source as a function of tissue-equivalent absorber thickness. Given the geometric mean or single-view uptake values, a five-compartment modeling analysis was performed (*32*) to estimate residence times for $^{111}$In and $^{90}$Y. Dose estimates for $^{90}$Y-cT84.66 were then estimated with the MIRD method (*33*) using the MIRDDOSE3 program (*34*).

Red marrow absorbed radiation dose estimates were possible in all 15 patients using the AAPM algorithm (*35*) based on the plasma clearance curves. For the nine patients on whom analyses of digitally stored nuclear images were performed, blood clearance curve fits were generated using the five-compartment model described above. For the remaining six patients, blood clearance curve fits were generated using a three-compartment model to fit of blood and urine data. Further details on the kinetic modeling and

**TABLE 1**
Patient Characteristics

| Primary no. | Age (yr) | Primary site | Histology | Serum CEA (ng/ml) | Disease extent |
|---|---|---|---|---|---|
| 1 | 67 | Rectum | Adenocarcinoma | 2.5 | 4.5 × 3.0-cm rectal mass; multiple liver metastses (largest 8 × 13 cm); 1.5 × 2.0-cm porta hepatis lymph node |
| 2 | 56 | Esophagus | Adenocarcinoma | 150 | 6 × 6-cm espohageal mass; 3 × 3-cm left supraclavicular lymph node; multiple 2–3-cm mediastinal lymph nodes; 3 × 5-cm gastric lymph node |
| 3 | 70 | Lung | Squamous cell carcinoma | 7.0 | 17 × 16-cm right lung mass; 3 × 3-cm left adrenal mass |
| 4 | 63 | Colon | Adenocarcinoma | 203 | Multiple hepatic metastases (largest, 7.3 × 3.3 cm); 3.5 × 3.7-cm right adrenal metastasis; 2.2-cm mediastinal lymph node; Multiple lung metastases (largest, 1.5 cm) |
| 5 | 70 | Thyroid | Medullary | 1034 | Multiple lung metastases (largest, 2 cm); multiple bone metastases (largest, 4.5 cm) |
| 6 | 24 | Thyroid | Medullary | 156 | Multiple cervical lymph node metastases (largest, 1.5 cm) |
| 7 | 51 | Rectum | Adenocarcinoma | <2.5 | 8 × 8-cm rectal mass |
| 8 | 72 | Colon | Adenocarcinoma | 3.9 | Multiple lung metastases (largest, 3.5 cm) |
| 10 | 35 | Breast | Infiltrating ductal carcinoma | 20 | Multiple bone metastases on bone scan (size not documented) |
| 11 | 59 | Breast | Infiltrating ductal carcinoma | 7.3 | Two 2-cm liver metastases; three bone metastases on bone scan (size not documented) |
| 13 | 76 | Colon | Adenocarcinoma | 120 | 7 × 7.2-cm anterior chest wall mass; multiple bone metastases on bone scan (size not documented) |
| 14 | 71 | Colon | Adenocarcinoma | 977 | 4.4 × 2-cm right adrenal mass; 1.3-cm lung mass; 1.2-cm mediastinal lymph node |
| 15 | 52 | Colon | Adenocarcinoma | 485 | 4.5 × 3-cm right adrenal mass; 7 × 5.5-cm left adrenal mass |
| 17 | 54 | Colon | Adenocarcinoma | 7.1 | 1.3 × 2.3-cm lung mass; 1.5-cm mediastinal lymph node |
| 18 | 70 | Lung | Squamous cell carcinoma | 228 | 6 × 10-cm left lung mass; multiple bone metastases (largest, 2 cm) |

dosimetry methods used can be found in a companion paper to this study by Odom-Maryon et al. (*32*).

All tumor dose estimates used a single uptake against time curve, as determined by serial images from one representative patient. Pathology specimens when available were used to define tumor volume and provided tissue counts to quantitate tumor uptake. Doses were estimated by integrating the point source function over the tumor volume. Edge effects were considered using a method previously published by this group (*36*).

## RESULTS

Eighteen patients were enrolled, of which 15 were evaluable for analysis. One patient did not receive antibody due to clinical deterioration, and one patient was infused with the antibody but did not return for any scans. A third patient was infused with the antibody based on elevated serum CEA levels by reports from the referral institution. However, tumor CEA expression could not be confirmed at this institution by either elevated serum CEA levels or by positive CEA immunohistochemistry staining of tumor tissue.

Table 1 lists the characteristics of all 15 patients. Eight patients were men and seven were women, with a median age of 62 yr (range, 36–76 yr). Seven patients had colorectal cancer, three had lung cancer, two had breast cancer, one had esophageal cancer and two had medullary thyroid cancer.

### Imaging Results

Fourteen of 15 patients (93%) had imaging of at least one known tumor site. Examples from four of these patients are presented in Figures 1–4. A total of 74 lesions was analyzed. The median number of lesions per patient was three with a range of 1–20. Sensitivity of the antibody scans was 45.1% (32 of 71), and PPV was 94.1% (32 of 34). Table 2 presents the imaging results for all lesions. All four primary tumors (two colorectal, one lung and one esophageal) were imaged with the chimeric antibody. Hepatic metastases were not imaged or seen as cold spots due to normal liver uptake and were scored as FNs.

Five (62.5%) of eight lymph node metastases seen on CT

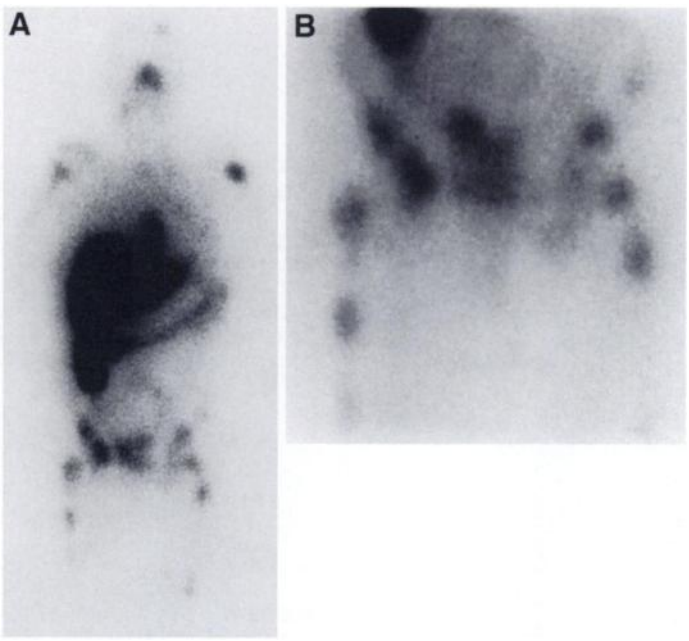


**FIGURE 1.** (A) Anterior whole-body view and (B) anterior spot pelvis view of a 64-yr-old woman with medullary thyroid cancer metastatic to bone (Patient 5) at 48 hr postinfusion. Antibody localization to metastases in the pelvis, bilateral femurs and shoulder regions was seen.

**FIGURE 2.** A 51-yr-old man with an 8 × 8-cm rectal adenocarcinoma (Patient 7). Antibody localization to the primary tumor was observed on the posterior whole-body view 48 hr postinfusion.

scan were imaged by the antibody. In addition, four patients demonstrated imaging of radiologically normal lymph nodes, which, in three patients, was felt secondary to CEA draining from nearby metastatic sites (Patients 7, 8 and 18). The fourth patient (Patient 14) had unusually slow antibody clearance and demonstrated nonspecific uptake to bilateral axillary and inguinal lymph nodes.

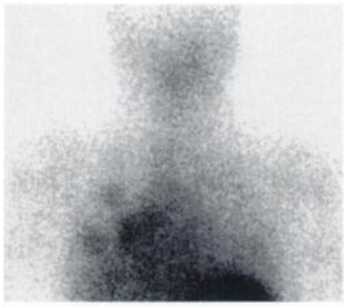

**FIGURE 3.** Antibody uptake was visualized in two left lung metastases on the 48-hr posterior spot chest view in a 72-yr-old woman with metastatic colon cancer (Patient 8). Antibody localization also was seen in left hilar lymph nodes. Tissue counts from biopsies of these nodes are reported in Table 3.

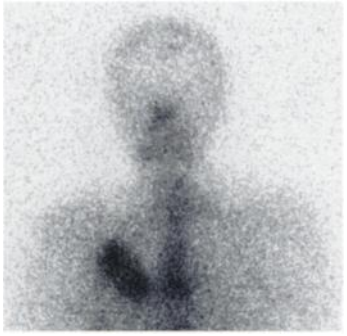

**FIGURE 4.** A 76-yr-old woman (Patient 13) with a 7 × 7.2-cm anterior chest wall metastasis from colorectal cancer. Antibody localization is demonstrated on the anterior spot chest view at 48 hr postinfusion.

Patients were followed for at least 6 mo after antibody infusion. During this period, one patient with medullary thyroid cancer (Patient 5) developed two additional bone metastases at sites that were originally felt to be FPs on antibody scan.

Tumor histologic type, extent of disease and preinfusion serum CEA level, which ranged from <2.5 to 1034 ng/ml, did not appear to influence antibody imaging. No side effects, changes in vital signs or changes in laboratory values were associated with antibody administration.

### Evaluation of Immunogenicity

All 15 patients were evaluated for HACA within the first month after antibody infusion, with 13 patients evaluated at 3 mo and 9 patients evaluated at 6 mo. One patient (Patient 13) developed a HACA response with measurable titers to cT84.66–DTPA (54.9 ng/ml) at 2 wk postinfusion. At 1 mo, titers had increased to 152.4 ng/ml. At 3 mo antibody titers to cT84.66–DTPA further increased (221 ng/ml), and antibodies to cT84.66 (114.8 ng/ml) were first detected. The patient expired from metastatic disease before the planned 6-mo blood sample. Competitive inhibition studies were performed to determine the site of HACA reactivity. mT84.66, mT84.66–DTPA and cT84.66–DTPA produced approximately 80%–100% inhibition, whereas normal human IgG–DTPA produced no inhibition of binding to cT84.66, suggesting that the antibody response was directed predominantly toward the murine portion and not the Fc portion of cT84.66. Ongoing studies are defining whether the HACA response was anti-idiotypic, and these results will be reported separately.

### Tissue Counts

Tissue counts were available from four patients who had exploratory surgery within 1–2 wk after antibody infusion (Table 3). Indium-111 uptake in one primary (Patient 7) and two metastatic (Patients 8 and 17) colorectal cancer lesions ranged from to 4.4% to 10.5% ID/kg. In a fourth patient (Patient 1), uptake was only 0.5% ID/kg in the primary tumor and 1.3% ID/kg in a histologically positive porta-hepatic lymph node, whereas uptake in liver metastases was higher (5.1 and 13.2% ID/kg). This patient demonstrated the fastest clearance of antibody to liver in the group (Fig. 5), possibly contributing to low uptake in the primary tumor and lymph node.

Tissue counts were not available for the eight lymph node metastases seen by CT scan and reported in Table 2. However, tissue counts were available from an enlarged porta-hepatic lymph node from Patient 1, which contained tumor on histologic examination. Tissue counts also were available from a separate set of clinically normal regional lymph nodes removed at surgery from three patients (peri-colonic lymph nodes in Patient 7 and hilar/mediastinal lymph nodes in Patients 8 and 17). Activity in these draining regional lymph nodes varied from 4.5% to 377% ID/kg (Table 3). All surgically sampled nodes from Patients 7, 8 and 17 were histologically negative for tumor on routine bisection and single section examination. Four lymph nodes from Patient 8 stained positive for CEA, primarily in sinus histiocytes.

### Pharmacokinetic Analysis and Dosimetry Estimates

Serum clearance rates were estimated for all 15 patients. Antibody cleared serum with a median $T_{1/2\alpha}$ of 6.53 hr (range, 0.31–43.36 hr) and $T_{1/2\beta}$ of 90.87 hr (range, 30.03–229.06 hr). A wide range of blood clearance rates was observed (Figs. 5 and 6). For all patients, the rate of clearance from blood was directly proportional to the rate of activity excreted in the urine. This is demonstrated in Figure 6, which compares blood residence time of $^{111}$In activity with residence times in urine and liver for the

**TABLE 2**
Imaging Results with Indium-111-Labeled cT84.66

| Type of lesion | No. sites analyzed | TP | FN | TN | FP | Sensitivity (%) | PPV (%) |
|---|---|---|---|---|---|---|---|
| All lesions | 74 | 32 | 39 | 1 | 2 | 45.1 (33.2–57.3) | 94.1 (80.3–99.3) |
| Primary tumor | 4 | 4 | 0 | 0 | 0 | 100 (47.3–100.0) | 100 (47.3–100.0) |
| Pulmonary lesion | 8 | 6 | 2 | 0 | 0 | 75.0 (34.9–96.8) | 100.0 (60.7–100.0) |
| Bone lesion | 41 | 15 | 24 | 0 | 2 | 38.5 (23.4–55.4) | 88.2 (63.6–98.5) |
| Hepatic lesion* | 6 | 0 | 6 | 0 | 0 | 0.0 (0.0–39.3) | |
| Adrenal lesion | 6 | 1 | 4 | 1 | 0 | 20.0 (0.4–57.9) | 100 (0.8–90.6) |
| Soft tissue lesion | 1 | 1 | 0 | 0 | 0 | 100 (5.0–100) | 100 (5.0–100) |
| Lymph node | 8 | 5 | 3 | 0 | 0 | 62.5 (24.5–91.5) | 100 (54.9–100) |

95% confidence intervals are in parentheses; Sensitivity = TP/(TP + FN); PPV = TP/(TP + FP).
*One of six lesions seen as cold area within the liver.

nine patients where data were fitted using the five-compartment model (*32*). Patients with faster blood clearance of activity, seen as lower blood residence time, demonstrated greater activity localizing to liver and clearing through the urine. Urine activity was seen as a low-molecular weight (5-kDa) metabolite on HPLC.

Blood clearance did not correlate with preinfusion serum CEA levels (Fig. 7). In all patients with detectable circulating antigen, CEA–antibody serum complexes were observed on size-exclusion HPLC analysis, with higher circulating CEA serum levels, resulting in a larger complex peak (Fig. 8). In patients with high liver accumulation, the CEA complexes cleared quickly from the serum, whereas in those patients with less hepatic accumulation, serum complexes persisted. Taken together, these data suggest that individual differences in antibody blood clearance kinetics were due to differences in hepatic clearance and metabolic rates of antigen–antibody complexes. Complexes localizing to liver were metabolized to a low-molecular weight metabolite that was excreted though the renal system.

Yttrium-90-cT84.66 radiation dose estimates to normal organs are given in Table 4. Differences between patients were primarily due to variations in the rate of antibody clearance from blood to liver as described above. Tumor dose estimates also were performed in five patients (Table 3). Four of these patients had exploratory surgery 7–14 days after antibody infusion and, therefore, tumor dimensions from pathologic specimens and $^{111}$In counts were available. In Patient 7 with a 8 × 8 × 8-cm primary rectal cancer, antibody uptake at 7 days postinfusion was 4.8% ID/kg. Tumor doses were estimated from uptake against time curves determined from serial nuclear images, resulting in an estimated dose of 10.1 cGy/mCi $^{90}$Y. In Patient 8, who had a surgically-resected lung metastasis, antibody uptake was 10.5% ID/kg. Assuming a time–activity curve similar to Patient 7 and scaling for uptake, a dose of 21.3 cGy/mCi $^{90}$Y was estimated. In a third patient (Patient 17), a dose of 12.8 cGy/mCi $^{90}$Y to a 1.7 × 1.0 × 1.0-cm surgically-resected lung metastasis was estimated from tissue biodistribution data and assuming a time–activity curve identical in shape to that of Patient 7 but scaled for uptake. In a fourth patient (Patient 13) with a chest wall metastasis, tissue counts from biopsies were not available but, as with Patient 7, tumor dimensions were measurable by CT scan and tumor images were clearly seen on all serial scans, allowing for adequate determination of time against uptake curves. Assuming tumor biodistribution as with Patient 7, a dose of 11.0 cGy/mCi $^{90}$Y was estimated for this 7.2 × 4.5 × 7-cm chest wall metastasis. Finally in Patient 1, who demonstrated very rapid clearance of antibody to liver, primary tumor uptake was low, resulting in a dose estimate of 0.97 cGy/mCi $^{90}$Y, again assuming a time–

**TABLE 3**
Indium-111 Activity in Resected Tumor and Regional Lymph Nodes

| Patient no. | Tumor size (greatest dimension, cm) | Tumor indium-111 activity (%ID/kg) | Tumor yttrium-90 dose (cGy/mCi) | Lymph node size (greatest dimension, cm) | Lymph node indium-111 activity (%ID/kg) | Lymph node yttrium-90 dose (cGy/mCi) |
|---|---|---|---|---|---|---|
| 1 | 4.5 (rectal primary) | 0.5 | 0.97 | 2.0 | 1.3 | 2.0 |
| | 2.5 (liver metastasis) | 3.0 | 5.1 | | | |
| | 13.0 (liver metastasis) | 6.6 | 13.2 | | | |
| 7 | 8.0 (rectal primary) | 4.8 | 10.1 | 0.7 | 4.5 | 4.5 |
| | | | | 0.8 | 35.3 | 57.4 |
| 8 | 3.5 (lung metastasis) | 10.5 | 21.3 | 1.0 | 6.8† | 9.1 |
| | | | | 0.7 | 29.4 | 29.5 |
| | | | | 0.6 | 50.7† | 46.8 |
| | | | | 1.0 | 92.1 | 122.7 |
| | | | | 0.7 | 208† | 209 |
| | | | | 0.8 | 377† | 617 |
| 17 | 1.7 (lung metastasis) | 4.4 | 12.8 | 0.5 | 67.0 | 89.2 |
| | | | | 1.3 | 14.0 | 34.5 |

*Positive for tumor on histologic examination.
†Carcinoembryonic antigen immunostaining performed. All lymph nodes stained positive (3+ on a scale of 1–4), with staining primarily in sinusoidal histiocytes.

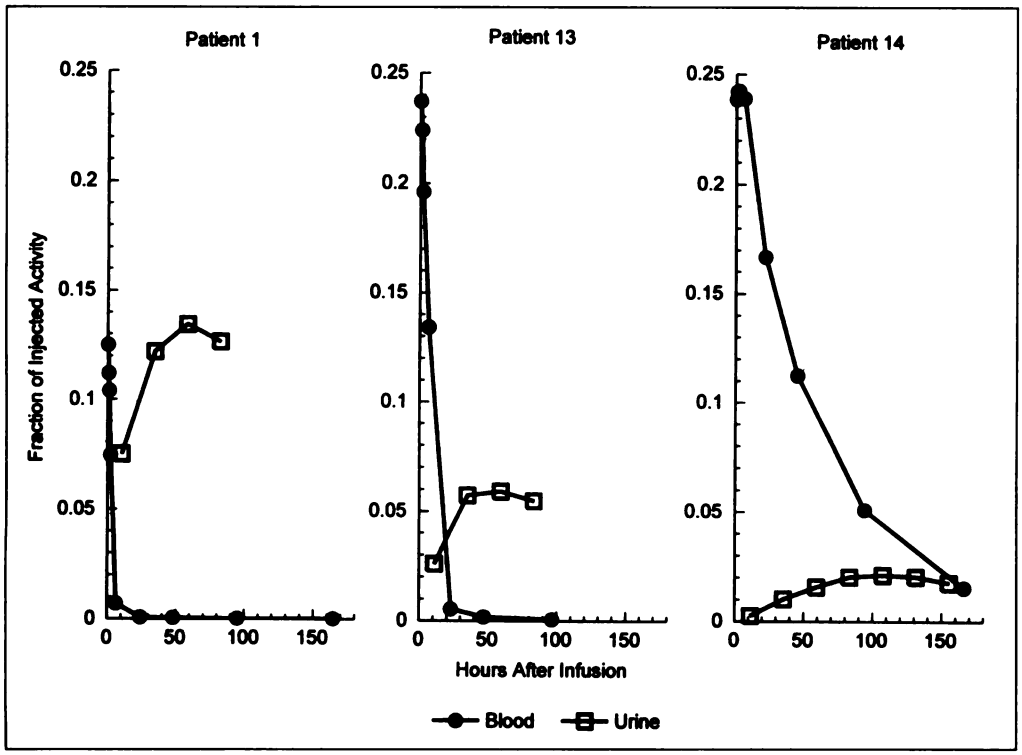


**FIGURE 5.** Blood (●) and urine (□) activity as a function of time postinfusion in three patients. Patient 1 demonstrated the fastest blood clearance of the 15 patients on this study, whereas Patient 14 demonstrated the slowest clearance. Patient 13 was representative of a moderately fast clearer. Patients demonstrating faster clearance of activity from the blood also demonstrated greater excretion of activity out through the urine as a low-molecular weight metabolite.

activity curve similar to that of Patient 7. Uptake to liver metastases was higher, with estimated doses of 5.1 and 13.2 cGy/mCi $^{90}$Y.

Yttrium-90-cT84.66 dose estimates were also performed for 11 regional lymph nodes that were surgically removed from the above patients, using the method described above (Table 3). Lymph nodes ranged in size from 0.5–2.0 cm and were porta-hepatic (Patient 1), peri-colonic (Patient 7) or mediastinal/hilar (Patients 8 and 17) in location. Given lymph node biodistributions between 1.3% and 377% ID/kg, dose estimates to lymph nodes ranged from 2 to 617 cGy/mCi $^{90}$Y.

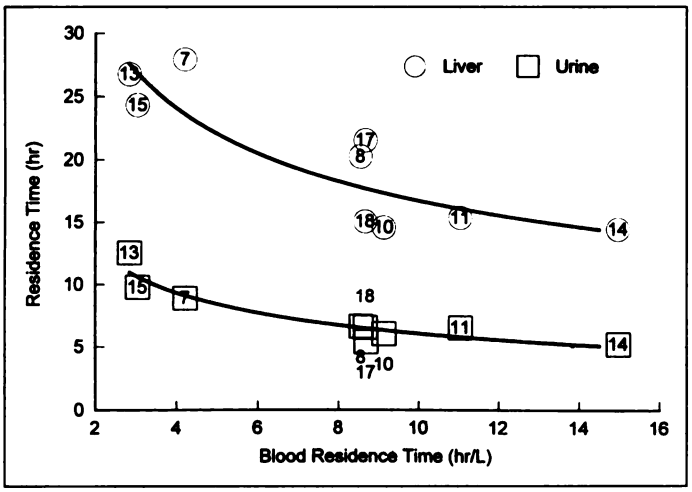


**FIGURE 6.** Indium-111 residence time in blood as a function of residence time in liver (○) and in urine (□). Patient number is shown in the center of each data point. The curves represent a power-law regression fit of the blood against liver data ($r = -0.858$) and of the blood against urine data ($r = -0.941$). Inverse correlations between blood and liver activity and between blood and urine activity were observed. For each patient, activity to liver correlated closely with activity excreted into the urine, suggesting that blood clearance was primarily dictated by the rate of activity cleared by the liver, with subsequent hepatic metabolism to a low-molecular weight metabolite excreted into the urine.

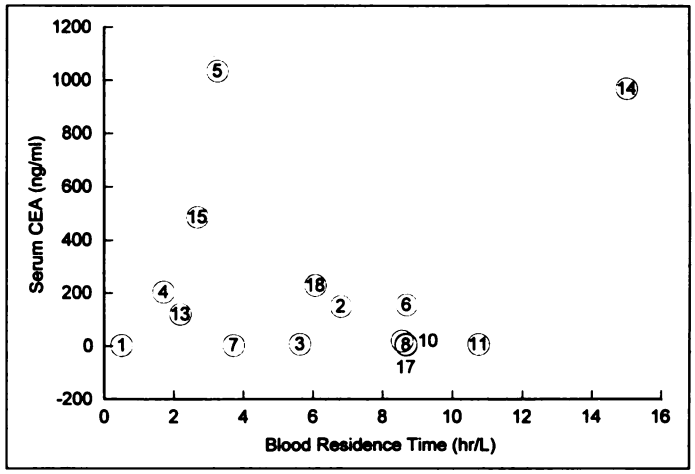


**FIGURE 7.** Indium-111 blood residence time as a function of preinfusion serum CEA level. Patient number is shown in the center of each data point. No correlation was observed between serum CEA and blood residence time.

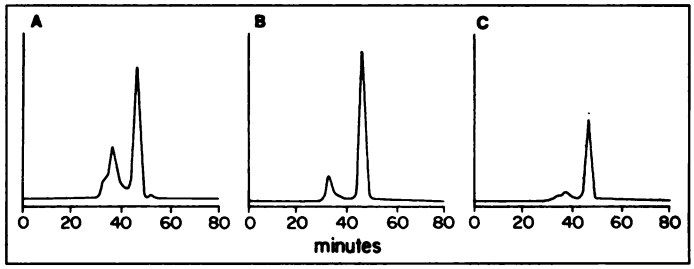


**FIGURE 8.** Size-exclusion HPLC tracings of serum samples at 2–6 hr post-antibody infusion from three patients administered cT84.66. (A) Serum CEA levels for Patient 5, 1034 ng/ml; (B) Patient 6, 156 ng/ml; and (C) Patient 7, 2.5 ng/ml (C). All three demonstrated a second smaller peak representing the formation of antibody–antigen complexes. The size of the peak correlated with the level of circulating CEA.

**TABLE 4**
Normal Organ Dosimetry with Yttrium-90-Chimeric T84.66

| Organ | Dosimetry (rod/mCi) | |
|---|---|---|
| | Average | Range |
| Lung | 1.75 | 1.09–2.31 |
| Liver | 24.1 | 15.0–37.1 |
| Spleen | 4.65 | 0.65–10.2 |
| Kidney | 2.81 | 0.29–5.34 |
| Red marrow | 2.37 | 0.77–3.54 |
| Total body | 2.35 | 1.55–2.78 |

## DISCUSSION

Radiolabeled murine Mabs have shown promise as agents for cancer imaging and therapy. However, HAMA formation in a significant percentage of patients who are administered murine antibodies limits multiple administrations (*16,17*). To reduce antibody immunogenicity, several groups have genetically engineered chimeric Mabs with most (*21,22*) but not all (*18*) murine antibodies, demonstrating reduced immunogenicity. The purpose of this study was to evaluate the immunogenicity and tumor-targeting properties of chimeric T84.66, an anti-CEA $IgG_1$ derived from murine T84.66.

Chimeric T84.66 retained high affinity ($1.16 \times 10^{11}\ M^{-1}$) and specificity to CEA as its murine antecedent. When radiolabeled with $^{111}$In and administered to patients with CEA-producing metastatic cancers, cT84.66 showed tumor targeting, with 100% (four of four) primary tumors imaged, 62.5% (five of eight) known lymph node metastases imaged and an imaging sensitivity rate of 45.1% and PPV of 94.1% (Table 2). As anticipated, hepatic and adrenal metastases were difficult to image due to normal liver uptake of activity. Bone metastases accounted for a significant fraction of the lesions, the majority of which were in two patients, Patient 5, with 20 bone lesions, and Patient 13, with 13 lesions. Although bone metastases in the pelvis and extremities were visualized (Fig. 1), more centrally located bone lesions, particularly those in the axial skeleton, were more difficult to image due to cardiac and hepatic activity. If bone lesions are excluded, imaging sensitivity would improve to 53.1%. If bone, adrenal and hepatic lesions are excluded, imaging sensitivity would increase to 75%.

Imaging results appear to be comparable to previously reported $^{111}$In intact anti-CEA Mabs (*16,37–39*). For example, the $^{111}$In-labeled anti-CEA murine monoclonal $IgG_1$ ZCE-025, when evaluated at this institution (*37*), demonstrated an imaging sensitivity of 40.5% and PPV of 83.1%. Divgi et al. (*16*), in a multi-institutional trial, reported a lesion detection rate of 56% with $^{111}$In-labeled C110, a murine $IgG_1$ against CEA, in patients with colorectal cancer.

Chimeric T84.66 cleared serum with a median $T_{1/2\alpha}$ of 6.53 hr (range, 0.31–43.36 hr) and $T_{1/2\beta}$ of 90.87 hr (range, 30.03–229.06 hr). Comparisons cannot be made with murine T84.66 because serum pharmacokinetic analyses were not reported from that imaging study. However, clearance kinetics were similar to that reported by Buchegger et al. (*22*), who evaluated a radioiodinated chimeric intact anti-CEA in 18 patients with colorectal cancer and reported a $T_{1/2\alpha}$ of 7.2 hr (range, 1.4–18.4 hr) and $T_{1/2\beta}$ of 91 hr (range, 30–292 hr).

A wide variation in serum clearance rates was observed, with an inverse correlation between blood and liver residence times observed (Fig. 6). Patients with greater localization of activity to liver demonstrated greater excretion of activity through the urine, indicating that the interpatient variability of antibody serum clearance was related to the rapidity of clearance of antigen–antibody complexes from blood to liver. Complexes once localized to liver were metabolized and excreted through the urine as a low-molecular weight (5-kDa) metabolite. Reasons for such interpatient variation in hepatic clearance and CEA trafficking, however, remain unexplained at this time.

Antibody clearance was not related to preinfusion levels of CEA (Fig. 7). Of interest are the two patients with the highest serum CEA levels. One demonstrated relatively fast clearance (Patient 5), whereas the other demonstrated the slowest clearance on this study (Patient 14), suggesting that serum CEA levels are determined by an interplay between the rates of CEA production and clearance.

These observations differ from those recently reported by Yu et al. (*40*), who noted increased clearance rates of $^{131}$I-COL-1, a murine monoclonal $IgG_{2a}$ anti-CEA, in patients with higher serum CEA levels and/or greater tumor burden. Why a similar correlation was not observed in this study is not clear, but the lack of correlation may be related to the greater heterogeneity of tumor types in our patient population, which included not only gastrointestinal malignancies but also lung, breast and thyroid malignancies.

With high-affinity Mabs, such as cT84.66, increased antigen complexation was anticipated, which potentially could compromise tumor targeting. However, as predicted from previous murine biodistribution studies (*41*), although murine T84.66 demonstrated higher liver uptake and lower blood uptake compared to lower-affinity anti-CEA Mabs, presumably due to greater complexation of CEA and clearance of these complexes to liver, tumor uptake was not compromised. In the current study, complexation with circulating CEA was observed (Fig. 8), but as in the murine studies, antibody uptake to tumor did not appear to be adversely affected because tumor biodistributions and imaging results with $^{111}$In-DTPA–cT84.66 were comparable to that of lower-affinity anti-CEA Mabs (*16,38,39,42*).

Immunogenicity after single administration of cT84.66 was reduced compared to murine Mabs, with 1 of 15 patients developing HACAs directed against the murine portion of the antibody. These results are similar to that reported by other groups (*19,20,22*). Other chimeric antibodies have been more immunogenic. Human antichimeric antibody was seen in 7 of 12 patients receiving a single administration of chimeric B72.3 (*18*). Low-level HACA titers were observed in six of eight patients receiving a single dose of chimeric NR-LU-13 (*43*). As in this study, HACA responses have been generally directed to the murine portion of the molecule (*18,20,21*).

Tumor uptake ranged from 0.5% to 10.5% ID/kg, which was comparable to that observed for other radiolabeled anti-CEA antibodies, evaluated at this institution (*42*) and at other institutions (*16,22*). In other ongoing trials evaluating $^{111}$In-labeled cT84.66, uptakes as high as 52% ID/kg in primary colorectal cancers have been observed. Buchegger et al. (*22*) noted similar tumor targeting in select patients with a radiodinated chimeric anti-CEA antibody. Uptake as high as 62.6% ID/kg was observed primarily in small tumor deposits, which would be predicted from animal models (*44*).

Five of eight radiologically enlarged lymph nodes were imaged by the antibody. Tissue counts were not available from these sites. Tissue counts were available from a separate set of regional lymph nodes removed at surgery (Table 3). Uptake in these nodes ranged from 1.3% to 377% ID/kg. All surgically sampled lymph nodes, with the exception of one (from Patient 1), were clinically nonsuspicious and histologically negative for tumor. CEA immunostaining was positive, primarily in sinusoidal histiocytes, in the four lymph nodes examined. False-

positive nodal uptake has been previously reported by this group (*37,45*) and is felt to be possibly secondary to filtering of CEA by antigen-processing macrophages. Others hypothesize that binding of $IgG_1$ to Fc receptors may be involved (*46*). Alternatively, antibody–CEA complexes may form at the tumor site and eventually drain to regional nodes. Cote et al. (*47*) have noted microscopic disease in up to 50% of lymph nodes that were initially felt to be FPs when histologic examination of multiple sections and immunohistologic cytokeratin staining were performed, indicating that, in many of these nodes, antibody may actually be targeting antigen-producing tumor cells instead of antigen alone.

Yttrium-90-DTPA–cT84.66 dose estimates to tumor and normal organs also were performed. Excluding the primary tumor from Patient 1, who demonstrated unusually rapid clearance and, therefore, low tumor uptake, estimated tumor doses ranged from 5.1 to 21.3 cGy/mCi $^{90}$Y. This is approximately 2–10 times greater than the average estimated marrow dose, which is expected to be the dose-limiting organ for radioimmunotherapy. Based on biodistributions from available lymph node biopsies, dose estimates to lymph nodes ranged from 2 to 617 cGy/mCi $^{90}$Y. Although these biopsied lymph nodes were histologically negative for tumor, it is reasonable to predict comparable radiation doses to tumor-involved lymph nodes, which are targeted by the antibody.

## CONCLUSION

Chimeric T84.66 demonstrated, in this pilot imaging trial, tumor-targeting and imaging properties comparable to other radiolabeled intact anti-CEA Mabs. Immunogenicity after single administration was lower compared to murine antibodies. These properties make cT84.66 or a lower-molecular weight, faster-clearing derivative attractive for further evaluation as an imaging agent. Its further evaluation in Phase I therapy trials is also warranted because dose estimates indicate that potentially therapeutic radiation doses can be delivered to select tumors and regional lymph nodes. Finally, a wide variation in the rate of antibody clearance was observed, with one patient demonstrating very slow clearance, resulting in the highest estimated marrow dose of the group, and one patient demonstrating unusually rapid clearance, resulting in poor antibody localization to tumor. Data from this study suggest that serum CEA levels, antibody–antigen complex clearance and, therefore, antibody clearance are likely to be influenced by both the production and clearance rates of CEA. This underscores the importance of further identifying and understanding those factors that influence antibody trafficking and clearance, to allow for optimal patient selection and rational planning of radioimmunotherapy.

## ACKNOWLEDGMENTS

We thank Lupe Ettinger, RN (protocol nurse); Gina Farino, BS (data manager); James Kao, MS, and Randall Woo, MS (radiopharmacy); George Lopatin, BS (dosimetry); Akiko Chai, MS (biostatistics); and Kathleen Thomas, CNMT, Ron Fomin, CNMT, and Joy Bright, CNMT (nuclear medicine) for their contributions. This work was supported by National Institutes of Health Grants PO1 43904, RO1 42329, T32 CA 09477 and Cancer Center Core Grant 33527 and by Deutsche Krebshilfe Dr.-Mildred-Scheel-Stiftung Grant W56/94/Ne2 (to M. N.).

## REFERENCES

1. Press OW, Eary JF, Appelbaum FR, et al. Radiolabeled-antibody therapy of B-cell lymphoma with autologous bone marrow support. *N Engl J Med* 1993;329:1219–1224.
2. Hird V, Maraveyas A, Snook D, et al. Adjuvant therapy of ovarian cancer with radioactive monoclonal antibody. *Br J Cancer* 1993;68:403–406.
3. Sheer DG, Schlom J, Cooper HL. Purification and composition of the human tumor-associated glycoprotein (TAG-72) defined by monoclonal antibodies CC49 and B72.3. *Cancer Res* 1988;48:6811–6818.
4. Kaminski MS, Zasadny KR, Francis IR, et al. Radioimmunotherapy of B-cell lymphoma with [131I]anti-B1 (anti-CD20) antibody. *N Engl J Med* 1993;329:459–465.
5. Esteban JM, Felder B, Ahn CA, Simpson JF, Battifora H, Shively JE. Prognostic relevance of carcinoembryonic antigen and estrogen receptor status in breast cancer patients. *Cancer* 1994;74:1575–1583.
6. Robbins PF, Eggensperger D, Qi CF, Schlom J. Definition of the expression of human carcinoembryonic antigen and non-specific cross-reacting antigen in human breast and lung carcinomas. *Int J Cancer* 1993;53:892–897.
7. Hansen HJ, Snyder LH, Miller E, et al. Carcinoembryonic antigen (CEA) assay. A laboratory adjunct in the diagnosis and management of cancer. *J Hum Pathol* 1974;5:139–147.
8. Abdel-Nabi HH, Schwartz AN, Higano CS, Wechter DG, Unger MW. Colorectal carcinoma: detection with $^{111}$indium anticarcinoembryonic antigen monoclonal antibody ZCE-025. *Radiology* 1987;164:617–621.
9. Divgi CR, McDermott K, Griffin TW, et al. Lesion-by-lesion comparison of computerized tomography and $^{111}$indium-labeled monoclonal antibody C110 radioimmunoscintigraphy in colorectal carcinoma: a multicenter trial. *J Nucl Med* 1993;34:1656–1661.
10. Goldenberg DM, Wlodkowski TJ, Sharkey RM, et al. Colorectal cancer imaging with iodine-123-labeled CEA monoclonal antibody fragments. *J Nucl Med* 1993;34:61–70.
11. Bischo-Delaloye A, Delaloye B. Diagnostic applications and therapeutic approaches with different preparations of anti-CEA antibodies. *Int J Biol Markers* 1992;7:193–197.
12. Stillwagon GB, Order SE, Haulk T, et al. Variable low dose rate irradiation ($^{131}$I-anti-CEA) and integrated low dose chemotherapy in the treatment of nonresectable primary intrahepatic cholangiocarcinoma. *Int J Radiat Oncol Biol Phys* 1991;21:1601–1605.
13. Beatty JD, Duda RB, Williams LE, et al. Pre-operative imaging of colorectal carcinoma with $^{111}$In-labeled anti-carcinoembryonic antigen monoclonal antibody. *Cancer Res* 1986;46:6494–6502.
14. Schroff RW, Foon KA, Beatty SM, Oldham RK, Morgan AC. Human anti-murine immunoglobulin responses in patients receiving monoclonal antibody therapy. *Cancer Res* 1985;45:879–885.
15. Courtenay-Luck LS, Epenetos AA, Moore R, et al. Development of primary and secondary immune responses to mouse monoclonal antibodies used in the diagnosis and therapy of malignant neoplasms. *Cancer Res* 1986;46:6489–6493.
16. Meredith RF, LoBuglio AF, Plott WE, et al. Pharmacokinetics, immune response and biodistribution of iodine-131-labeled chimeric mouse/human IgG1, k17-1A monoclonal antibody. *J Nucl Med* 1991;32:1162–1168.
17. Pimm MV, Perkins AC, Armitage NC, Baldwin RW. The characteristics of blood-borne radiolabelled antibodies and the effect of anti-mouse IgG antibodies on localization of radiolabeled monoclonal antibody in cancer patients. *J Nucl Med* 1985;26:1011–1023.
18. Khazaeli MB, Saleh MN, Liu TP, et al. Pharmacokinetics and immune response of 131I-chimeric mouse/human B72 3 (human gamma 4) monoclonal antibody in humans. *Cancer Res* 1991;51:5461–5466.
19. Handgretinger R, Anderson K, Lang P, et al. A phase I study of human/mouse chimeric anti-ganglioside GD2 antibody ch14 18 in patients with neuroblastoma. *Eur J Cancer* 1995;31A:261–267.
20. LoBuglio AF, Wheeler RH, Tranf J, et al. Mouse-human chimeric monoclonal antibody in man: kinetics and immune response. *Proc Natl Acad Sci USA* 1989;86:4220–4224.
21. Goodman GE, Hellstrom I, Yelton DE, et al. Phase I trial of chimeric (human-mouse) monoclonal antibody L6 in patients with non-small-cell lung, colon, and breast cancer. *Cancer Immunol Immunother* 1993;36:267–273.
22. Buchegger F, Mach JP, Pelegrin A, et al. Radiolabeled chimeric anti-CEA monoclonal antibody compared with the original mouse monoclonal antibody in surgically treated colorectal carcinoma. *J Nucl Med* 1995;36:420–429.
23. Wagener C, Clark BR, Rickard KJ, Shively JE. Monoclonal antibodies for carcinoembryonic antigen and related antigens as a model system: determination of affinities and specificities of monoclonal antibodies by using biotin-labeled antibodies and avidin as precipitating agent in a solution phase immunoassay. *J Immunol* 1983;130:2302–2307.
24. Wagener C, Yang YHJ, Crawford FG, Shively JE. Monoclonal antibodies for carcinoembryonic antigen and related antigens as a model system: a systematic approach for the determination of epitope specificities of monoclonal antibodies. *J Immunol* 1983;130:2308–2315.
25. Hefta LJ, Wu AM, Neumaier M, Shively JE. Measuring antibody affinity using biosensors. In: Chiswell D, MacCafferty J, Hoogenboom H, eds. *Antibody engineering: a practical approach*. London: Oxford Press; 1995:99–117.
26. Sumerdon, GA, Rogers, PE, Lombardo, CM, et al. An optimized antibody-chelator conjugate for imaging of carcinoembryonic antigen with $^{111}$indium. *Nucl Med Biol* 1990;17:247–254.
27. Neumaier M, Shively L, Chen FS, et al. Cloning of the genes for T84 66, an antibody that has a high specificity and affinity for carcinoembryonic antigen, expression of chimeric human/mouse T84 66 genes in myeloma and Chinese hamster ovary cells. *Cancer Res* 1990;50:2128–2134.
28. Wong JYC, Williams LE, Yamauchi DM, et al. Initial experience evaluating $^{90}$yttrium radiolabeled anti-CEA chimeric T84 66 in a Phase I radioimmunotherapy trial. *Cancer Res* 1995;55(suppl):5929s–5934s.
29. Williams LE, Primus FJ, Wong JYC, et al. Biodistribution of an In-111 or Y-90 labeled chimeric anti-CEA monoclonal antibody (cT84 66) following its large scale production in a bioreactor. *Tumor Targeting* 1996;2:116–124.
30. Galen RS, Fink DJ. Probabilistic approaches to clinical decision support. In: *Computer aids to clinical decisions*, Vol. 2. Boca Raton, FL: CRC Press, Inc; 1982:7–10.

31. D'Argenio DZ, Schumitzky A. A program package for simulation and parameter estimation in pharmacokinetic systems. *Comput Prog Biomed* 1979;9:115–134.
32. Odom-Maryon TL, Chai A, Williams LE, et al. Pharmacokinetics and modeling of cT84.66 chimeric anti-CEA antibody in humans. *J Nucl Med*; in press.
33. Loevinger R, Berman M. MIRD Pamphlet No. 1, Revised. New York: Society of Nuclear Medicine; 1976.
34. Stabin MG. MIRDOSE: personal computer software for internal dose assessment in nuclear medicine. *J. Nucl Med* 1996;37:538–546.
35. Siegel JA, Wessels BW, Watson EE, et al. Bone marrow dosimetry and toxicity for radioimmunotherapy. *Antibody Immunoconj Radiopharm* 1990;3:213–233.
36. Buras RB, Williams LE, Beatty BG, Wong JYC, Beatty JD, Wanek PM. A method including edge effects for the estimation of radioimmunotherapy absorbed doses in the tumor xenograft model. *Med Phys* 1994;21:287–292.
37. Corbisiero RM, Yamauchi DM, Williams LE, et al. Comparison of immunoscintigraphy and computerized tomography in identifying colorectal cancer: individual lesion analysis. *Cancer Res* 1991;51:5704–5711.
38. Patt YZ, Lamki LM, Haynie TP, et al. Improved tumor localization with increasing dose of indium-111-labeled anti-carcinoembryonic antigen monoclonal antibody ZCE-025 in metastatic colorectal cancer. *J Clin Oncol* 1988;8:1220–1230.
39. Patt YZ, Lamki LM, Shanken J, et al. Imaging with indium-111-labeled anticarcinoembryonic antigen monoclonal antibody ZCE-025 of recurrent colorectal or carcinoembryonic antigen-producing cancer in patients with rising serum carcinoembryonic antigen levels and occult metastases. *J Clin Oncol* 1990;8:1246–1254.
40. Yu B, Carrasquilo J, Milenic D, et al. Phase I trial of iodine 131-labeled COL-1 in patients with gastrointestinal malignancies: influence of serum carcinoembryonic antigen and tumor bulk on pharmacokinetics. *J Clin Oncol* 1996;6:1798–1809.
41. Beatty BG, Beatty JD, Williams LE, Paxton RJ, Shively JE, O'Connor-Tressel M. Effect of specific antibody pretreatment on liver uptake of $^{111}$In-labeled anticarcinoembryonic antigen monoclonal antibody in nude mice bearing human colon cancer xenografts. *Cancer Res* 1989;49:1587–1594.
42. Williams LE, Beatty BG, Beatty JD, Wong JYC, Paxton RJ, Shively JE. Estimation of monoclonal antibody-associated $^{90}$Y activity needed to achieve certain tumor radiation doses in colorectal cancer patients. *Cancer Res* 1990;50(suppl):1029s–1030s.
43. Weiden PL, Breitz HB, Seiler CA, et al. Rhenium-186-labeled chimeric antibody NR-LU-13: pharmacokinetics, biodistribution and immunogenicity relative to murine analog NR-LU-10. *J Nucl Med* 1993;34:2111–2119.
44. Williams LE, Duda RB, Proffitt RT, et al. Tumor uptake as a function of tumor mass: a mathematical model. *J Nucl Med* 1988;29:103–109.
45. Kuhn JA, Corbisiero RM, Buras RR, et al. Intraoperative gamma detection probe with presurgical antibody imaging in colorectal cancer. *Arch Surg* 1991;126:1398–1403.
46. Epenetos AA. Antibody guided lymphangiography in the staging of cervical cancer. *Br J Cancer* 1985;51:805–808.
47. Cote RJ, Houchens DP, Hitchcock CL, et al. Intraoperative detection of occult colon cancer micrometastases using $^{125}$I-radiolabeled monoclonal antibody CC49. *Cancer* 1996;77:613–620.

# Pharmacokinetic Modeling and Absorbed Dose Estimation for Chimeric Anti-CEA Antibody in Humans

Tamara L. Odom-Maryon, Lawrence E. Williams, Akiko Chai, George Lopatin, An Liu, Jeffrey Y.C. Wong, Jeffrey Chou, Kenneth G. Clarke and Andrew A. Raubitschek

*Departments of Biostatistics and Radioimmunotherapy and Divisions of Radiology and Radiation Oncology, City of Hope National Medical Center, Duarte, California, and Department of Radiological Sciences, University of California at Los Angeles Medical Center, Los Angeles, California*

The objective of this article was to model pharmacokinetic data from clinical diagnostic studies involving the $^{111}$In-labeled monoclonal antibody (MAb) chimeric T84.66, against carcinoembryonic antigen. Model-derived results based on the $^{111}$In-MAb blood, urine and digital imaging data were used to predict $^{90}$Y-MAb absorbed radiation doses and to guide treatment planning for future therapy trials. Fifteen patients with at least one carcinoembryonic antigen-positive lesion were evaluated. We report the kinetic parameter estimates and absorbed $^{111}$In-MAb dose and projected $^{90}$Y-MAb doses for each patient as well as describe our approach and rationale for modeling an extensive set of pharmacokinetic data. **Methods:** The ADAPT II software package was used to create three- and five-compartment models of uptake against time in the patient population. The "best-fit" model was identified using ordinary least squares. Areas under the curve were calculated using the modeled curves and input into MIRDOSE3 to estimate absorbed radiation doses for each patient. **Results:** A five-compartment model best described the liver, whole body, blood and urine data for a subcohort of nine patients with digital imaging data. A three-compartment model best described the blood and urine data for all 15 clinical patients accrued in the clinical trial. For the subcohort, the largest projected $^{90}$Y-MAb doses were delivered to the liver (mean, 24.78 rad/mCi; range, 15.02–37.07 rad/mCi), with red marrow estimates on the order of 3.32 rad/mCi (range, 1.24–5.55) of $^{90}$Y. Corresponding estimates for the $^{111}$In-MAb were 3.18 (range, 2.09–4.43) and 0.55 (range, 0.34–0.74), respectively. **Conclusion:** The three- and five-compartment models presented here were successfully used to represent the blood, urine and imaging data. This was evidenced by the small standard errors for the kinetic parameter estimates and $R^2$ values close to 1. As planned future therapeutic trials will involve stem cell support to alleviate hematological toxicities, the development of an approach for estimating doses to other major organs is crucial.

**Key Words:** compartmental models; anti-CEA; chimeric antibody; dose estimation

**J Nucl Med 1997; 38:1959–1966**

Monoclonal antibodies (MAbs) have had multiple clinical applications in both diagnostic (*1–3*) and therapeutic (*4–6*) nuclear medicine. Originally, most of these agents were murine antibodies generated by injecting normal mice with human tumor cells or other human proteins of interest. In the case of serial studies in the same patient, however, the use of such murine antibodies has typically led to the induction of a human antimouse antibody response (*7,8*). Others have suggested that the use of chimeric antibodies should reduce the incidence of human antiprotein responses (*9,10*). In this strategy, two-thirds of the murine IgG molecule is replaced with the corresponding human sequences by using recombinant DNA technology. Because the patient is less likely to develop a human antichimeric antibody response, the potential for serial therapeutic infusions is increased. As the use of chimeric molecules could result in changes in the human pharmacokinetics (PK), determination of a mathematical model describing the biodistribution of the antibody in the human system is desirable. Molecular changes in the MAb could then be correlated with variations in the model parameter estimates.

Although mathematical modeling has had a long association with the study of radiotracers (*11*), the application of modeling in clinical studies of antibodies has been much less extensive (*9,10,12*). A fundamental goal of such analyses is to establish a set of parameters that describe the distribution of a radiolabeled

Received Apr. 18, 1996; revision accepted Dec. 10, 1996.
For correspondence or reprints contact: Tamara L. Odom-Maryon, PhD, Department of Biostatistics, City of Hope, 1500 E. Duarte Rd, Duarte, CA 91010.